To cite this article: Ramiaramanana, F. N., Munyi, Jm.M, Archambeau, P., Teller, J. (2025). A comparative assessment of flood mapping methods for urban risk management in data-poor environments. Nat Hazards (2025). https://doi.org/10.1007/s11069-025-07590-9.

A comparative assessment of flood mapping methods for urban risk management in data-poor environments

Abstract

Flood mapping is essential to urban resilience, but it often relies on traditional hydrological models, which are poorly suited to data-scarce contexts due to their complexity and input requirements. This study, conducted in Antananarivo, Madagascar, evaluates alternative approaches combining remote sensing (Pleiades and Sentinel-1), simplified hydrological modeling (Fast Flood Simulation—FFS), and multicriteria analysis (MCA), with validation from field observations. The results show contrasting performances: FFS (10 cm threshold) detected 45% of flooded zones in the urban center, while Sentinel-1 identified only 3% due to poor performance in dense built-up areas. Pleiades was also affected by structural artifacts, despite its high resolution. MCA identified 40% of the city as being highly vulnerable. In agricultural zones, FFS captured over 80% of flooded areas, compared to 56% for MCA and less than 10% for Sentinel-1. In residential neighborhoods, flooded building detection ranged from under 1% (Sentinel-1) to 27% (FFS) and 37% (MCA). Overall, FFS emerged as the most suitable tool, providing flood depth estimates for operational decision-making, but its reliability depends heavily on input data quality and calibration processes. Satellite imagery offers complementary post-crisis validation but remains limited in dense urban environments. MCA supports strategic planning but cannot model event-specific dynamics. Combined within a GIS platform or interactive dashboard, these tools provide complementary capabilities across risk management

phases—prevention (FFS, remote sensing, MCA), crisis response (FFS), and reconstruction (FFS, remote sensing)—offering decision-support solutions adapted to data-poor environments.

Keywords

Flood mapping; Remote sensing; Fast Flood Simulation; Multicriteria analysis; Data-poor environments; Antananarivo

1. Introduction

Floods rank among the most widespread and devastating natural hazards globally, affecting millions of individuals each year and resulting in substantial human, economic, and environmental losses (CRED 2024). Their intensification is exacerbated by various factors, such as climate change, which affects the frequency and intensity of precipitation (Hirabayashi et al. 2013; Arnell and Gosling 2016; Tabari 2020), and rapid urbanization, which significantly modifies territories' landscapes and hydrological dynamics (McGrane 2016; Janicka and Kanclerz 2022; Sjöstrand 2022; Li et al. 2024). In urban areas, demographic concentration and surface sealing increase the risk of floods, particularly in regions where urban planning fails to keep pace with population growth (Suarez 2002; Doocy et al. 2013; Beshir and Song 2021; Wu et al. 2021). Notably, in many Global South countries, these transformations are occurring against a backdrop of significant institutional, economic, and technical constraints (Cohen 2006; Sridhar and Mavrotas 2021). Poorly managed urbanization often results in the expansion of informal settlements in vulnerable areas. (Williams et al. 2018; O'Sullivan 2022; Quesada-Román 2022; Anwana and Owojori 2023). The absence of adequate drainage infrastructure and flood evacuation facilities increases exposure to extreme events (Douglas et al. 2008; Rentschler et al. 2022; Ogbonna 2023), while fragmented governance and limited resources hinder effective risk management (Fatti and Patel 2013; Rentschler et al. 2022). This vulnerability is particularly critical in environments where land pressure and lack of planning lead populations to settle in flood-prone areas (Diop et al. 2017; Abunyewah et al. 2018; Ramiaramanana and Teller 2021). The consequences of these factors extend beyond material damage and directly impact living conditions, resulting in population displacement, loss of livelihoods, and health crises associated with water contamination (Shrestha and Takara 2008; Baker 2012; Chen et al. 2015; Kakinuma et al. 2020).

In the face of these challenges, flood mapping serves as a strategic lever for enhancing risk management, and identifying the most vulnerable areas helps to guide land use planning policies (Gashaw and Legesse 2011; Zakaria et al. 2017; Vojtek and Vojteková 2018; Janizadeh et al. 2021). The development of flood maps plays a central role in three key areas—prevention, by enabling the anticipation and reduction of risks; crisis response, by facilitating the early detection of floods and the coordination of relief efforts; and post-disaster planning, by providing actionable data for reconstruction and the reduction of long-term vulnerability (Merz et al. 2007; Herrero et al. 2009; Chen et al. 2011; Zakaria et al. 2017; Minano and Peddle 2018; Mudashiru et al. 2021; Rahman et al. 2024).

Flood mapping can be based on advanced hydrological and hydraulic models that are recognized for their efficiency (Brunner 1997; Arnold and Fohrer 2005; Jaber and Shukla 2012; Park and Markus 2014; Li et al. 2019; Mudashiru et al. 2021). However, the application of these models is often limited in contexts where data are insufficient, fragmentary, or of low quality, and where resources are restricted (Park and Markus 2014; Devi et al. 2015; Rahman and Di 2017; Kumar et al. 2023). Requirements for detailed hydrological parameters, long time-series data, sensitivity to local conditions, and high computational demands constrain the implementation of these models (Park and Markus 2014; Devi et al. 2015). These methodological challenges reduce the transferability of conventional models and underscore the need to develop alternative approaches that are better suited to data-poor environments.

Several approaches have been developed to address the limitations of these models. Most notably, remote sensing has opened up new avenues for detailed and continuous flood monitoring, while enabling large-scale mapping without requiring highly accurate inputs or complex calculations (Lin et al., 2016; Mudashiru et al., 2021; Munawar et al., 2022; Tanim et al., 2022; Sadiq et al., 2023). Very-high-resolution satellite imagery provides accurate data on surface water and flood extent (Shamaoma et al. 2006; Yésou et al. 2015; Rahman and Di 2017; Bhatt et al. 2020; Mukhopadhyay et al. 2024). However, optical imagery remains limited under cloud cover, restricting its use during extreme events (Lin et al. 2016; Tavus et al. 2020; McCormack et al. 2022). Radar imagery, which is insensitive to weather conditions, offers a robust alternative for the real-time detection of flooded surfaces (Twele et al. 2016; Anusha and Bharathi 2020; Nkwunonwo et al. 2020; McCormack et al. 2022; Nazir et al. 2023).

Simplified hydrological models have been developed to complement satellite data, addressing data availability constraints (Hunter et al. 2007; Teng et al. 2017). Fast Flood Simulation (FFS), a tool recently developed by Van den Bout et al. (2023), offers accessible flood modeling (Watson et al. 2024). Unlike sophisticated hydraulic models that solve the full dynamic equations governing water flow, FFS relies on a steady-state assumption, ignoring transient dynamics. It employs a fast-sweeping algorithm for hydrological terrain correction and flow accumulation, significantly reducing computational time—it operates over 1,500-times faster than conventional models (Van den Bout et al., 2023). This flexible approach facilitates the identification of vulnerable areas and the development of adaptation strategies, particularly in regions where hydraulic data and modeling tools are not widely accessible (Glas 2023).

Beyond simplified flood simulation, multicriteria analysis (MCA) offers an alternative method for assessing flood susceptibility (Liuzzo et al., 2019; Saleh et al., 2020). This approach relies on weighting and prioritizing multiple factors, including topographic features, hydrological variables, land use, and precipitation (Khosravi et al., 2019; Handini et al., 2021). Rather than modeling hydrological processes, this method establishes a classification of vulnerabilities, thus facilitating the identification of the most exposed areas (Papaioannou et al. 2015).

Although flood mapping tools have been enhanced by technological advances, their use remains limited due to the absence of objective analysis concerning their complementarity and integration into a comprehensive flood management strategy (Devi et al. 2015; Lin et al. 2016; Mudashiru et al. 2021; Kumar et al. 2023). This fragmentation underscores the necessity for thorough benchmarking, considering data availability, model performance, and their impact on decision-making. For comparability, Table 1 provides a summary of these flood assessment methods, highlighting their data requirements, types of results, and contributions to flood management.

Table 1. Overview of flood mapping methods and their management applications

Method	Data requirements	Types of results	Application in flood management	References
Remote sensing	Optical and radar satellite imagery	- Flood extent - Temporal evolution of flood-prone areas	- Monitoring at-risk areas - Crisis response assistance - Validation of hydrological models	Yésou et al. 2015; Twele et al. 2016; Amitrano et al. 2018; McCormack et al. 2022; Nhangumbe et al. 2023
Simplified hydrological model: FFS	Digital Elevation Model (DEM), precipitation, surface roughness, infiltration rate	- Simulated flood extent - Water depth estimation	- Support for operational and strategic decisions	Glas 2023; Van den Bout et al. 2023
MCA	Multiple variables: topography, precipitation, land use, hydrographic network, etc.	- Vulnerability ranking - Flood susceptibility assessment	- Support for risk planning and management - Orientation of preventive measures and interventions	Khosravi et al. 2019; Handini et al. 2021

To identify the most robust methods, their complementarity and operational potential for data-poor environments, this study describes a comparative assessment of the leading flood mapping methods combining optical and radar remote sensing, simplified flood modeling, and MCA. Antananarivo, Madagascar, described as emblematic of the challenges associated with flooding in resource-poor urban environments (Ramiaramanana and Teller 2021; Rakotoarimanana and Rakotovao 2022), is used as a relevant case study to test these different methods in a real-world context, with a focus on their practical contribution to risk management decision-making.

2. Study area

The Antananarivo agglomeration, also known as Greater Antananarivo (GT), the capital of Madagascar, spans approximately 76,800 hectares and had an estimated population of 3.3 million in 2022 (Institut National de la Statistique—INSTAT). At its core, the Commune Urbaine d'Antananarivo (CUA) lies in a low-lying basin (1,242–1,261 m above sea level), punctuated by hills that shape local drainage patterns (Fig. 1a). To the west, a gently sloping plain forms a hydraulic convergence zone, increasing flood vulnerability due to flow accumulation near key river channels (Rambinintsoa 2012; ARTELIA 2014).

The hydrographic network surrounding the CUA amplifies flood risk, particularly in low-lying areas where outdated, undersized, or clogged drainage infrastructure—often obstructed by waste and debris—limits the absorption of runoff (ARTELIA 2014; Ciampalini et al. 2019). Rapid urban expansion in recent decades has increased impervious surfaces, disrupting natural infiltration (Rambinintsoa 2012; Dupuy et al. 2023). Land use data from 2022 indicate growing densification in the CUA, with the remaining green spaces primarily confined to the southern and eastern hills (Fig. 1b). Peri-urban communes are undergoing accelerated conversion to residential and industrial zones, intensifying surface runoff (Olisoa 2012; Attoumani et al. 2019). Downstream rural areas, which are predominantly agricultural, remain highly vulnerable to flood hazards (Defrise et al. 2017).

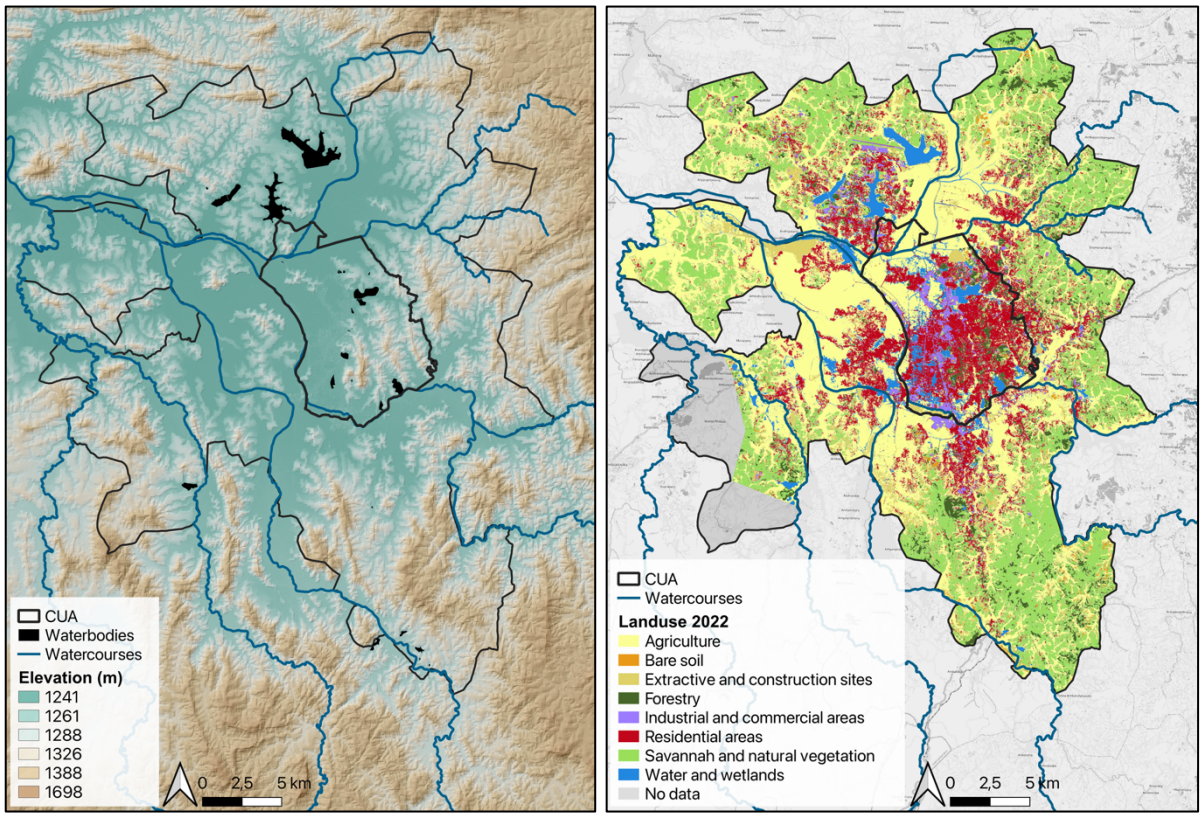

a. Topography b. Landuse in 2022

Fig. 1. Study area

Data sources: European Space Agency (ESA); Centre de coopération Internationale en Recherche Agronomique pour le Développement (CIRAD); Autorité pour la Protection contre les Inondations de la Plaine d'Antananarivo (APIPA).

Rainfall in the study area is highly seasonal, concentrated between November and March, with January and February typically being the wettest months. Combined with rapid soil saturation, these conditions substantially increase flood potential (Ciampalini et al. 2019; Rakotoarimanana and Rakotovao 2022).

3. Data and methodology

Three distinct approaches to flood mapping were explored, namely remote sensing data analysis, the FFS model, and MCA. Each method offers a distinct perspective, leveraging different data sources and analytical techniques.

Table 2 provides an overview of the key datasets used in this study and their sources and scales. Further details are available in Online Resource 1—Part 1.

Table 2. Data used in this study to conduct flood risk modeling using different methodological approaches

	Data	Scale / Source	Accessibility
Aerial imagery	Pleiades image—2 m resolution 28/01/2022	CUA / ESA	Licensed or on request
Radar imagery	Sentinel-1 image—10 m resolution 27/01/2022	GT / ESA	Open access
FFS	Surface roughness (Manning coeff.)	GT / ESA	Open access
	Infiltration rates	GT / SoilGrids	Open access
	Daily precipitation per hour 24/01/2022	GT / APIPA	Local data—on request
MCA	DEM—30 m resolution	GT / ESA	Open access
	Monthly precipitation from 2010 to 2021	GT / WorldClim	Open access
	Hydrographic network: watercourses	GT / APIPA	Local data—on request
	Lithology: lithological map 2020	GT / SGMA	Local data—on request
	Landsat image—30 m resolution 29/08/2022	GT / NASA; USGS	Open access
Impact assessment	Landuse—2022	GT / CIRAD	Open access
	Openbuilding data—2022	GT / Google Building	Open access
Validation	Areas affected by flooding—2023	CUA / Focus groups with local experts	On request

Note: CUA = Commune Urbaine d'Antananarivo; GT = Greater Antananarivo; ESA = European Space Agency; APIPA = Autorité pour la Protection contre les Inondations de la Plaine d'Antananarivo; SGMA = Service Géologique et des Mines d'Antananarivo; CIRAD = Centre de coopération Internationale en Recherche Agronomique pour le Développement; NASA = National Aeronautics and Space Administration; USGS = United States Geological Survey.

All datasets were processed using the EPSG:32738 coordinate reference system (WGS 84 / UTM Zone 38S).

3.1. Observed flood mapping using Pleiades aerial imagery—CUA scale

Flood extent information was extracted from a 2 m resolution Pleiades image acquired on 28/01/2022. The image presented minimal cloud cover and high spatial detail, enabling accurate detection of inundated areas in dense urban settings. This type of data is particularly valuable in data-scarce environments, where detailed geospatial information is often lacking (Rahman and Di 2017).

An Object-Based Image Analysis (OBIA) approach was adopted to enhance flood detection in dense urban settings by leveraging the spectral, spatial, and textural characteristics of image segments (Blaschke 2010; Dao et al. 2019). The segmentation process was followed by supervised classification using a Support Vector Machine (SVM) trained on 1,400 manually labeled samples. Manual corrections were made by cross-referencing with building vector data. All analyses were conducted using QGIS version 3.34.9.

3.2. Observed flood mapping using Sentinel-1 radar imagery—GT scale

Owing to its free accessibility and frequent revisit cycle, Sentinel-1 data is especially valuable for large-scale flood monitoring in regions with limited data availability. A Sentinel-1 SAR image (10 m resolution, 27/01/2022) was used to detect surface water, benefiting from weather- and light-independent acquisition (McCormack et al. 2022). VV polarization is preferred due to its greater sensitivity to surface water, which appears darker in radar images because of lower backscatter (Twele et al. 2016; McVittie 2019a; Mohamadiazar et al. 2024). The preprocessing stages carried out included radiometric calibration, speckle filtering, and terrain correction (Denis 2019; McVittie 2019b). Flood classification was performed using manual thresholding based on backscatter histograms. All processing steps were performed using the Sentinel Application Platform (SNAP), version 10.0.0, developed by the European Space Agency (ESA).

3.3. Simulated flood-prone areas mapping using the FFS model—GT scale

The FFS model estimates peak flows and water depths under quasi-steady conditions, assuming equilibrium between inflow and outflow across the watershed (Van den Bout et al. 2023). This approach reduces computational demands while remaining well suited to flood hazard assessment (Glas 2023; Van den Bout et al. 2023).

The inputs to this model include rainfall intensity, soil infiltration, surface roughness (Manning coefficient), and a DEM corrected via the Fast Sweeping Method (FSM), which removes depressions and ensures a consistent downslope gradient (Zhao 2005; Van den Bout et al. 2023). The hydrologically corrected DEM is then used to simulate steady-state flow across the catchment. Unlike iterative routing, the FSM propagates flow in a single pass, enhancing efficiency while preserving accuracy (Van den Bout et al. 2023). Rainfall is assumed to be uniform and constant, a necessary simplification due to the limited data available, and discharge is calculated for each grid cell based on the upslope area and rainfall intensity. Water depth is derived by inverting the kinematic form of Manning's equation.

To address spatial heterogeneity and limitations associated with uniform discharge assumptions, the model integrates a compensation scheme based on catchment structure; it estimates the local flow equilibrium using an exponential relationship between the contributing area and distance to the outlet. Rather than simulating temporal variations directly, spatial proxies, such as the estimated travel time, are used to approximate the interaction between rainfall duration and catchment concentration time (Van den Bout et al. 2023). A diffusive wave solver then adjusts the final water surfaces using slope, friction, and gravity to enhance realism without requiring complete dynamic modeling (Van den Bout et al. 2023).

Four simulation scenarios were carried out using the online FastFlood App (https://fastflood.org/) by varying the infiltration rates and surface roughness to calibrate the model (see Online Resource 1—Part 2). Water depths were classified according to local flood thresholds (Lambert et al. 2017; Labatte et al. 2018), and a sensitivity analysis was performed by excluding depths below 0.10 m and 0.25 m. The impact of the hydrological correction was then assessed by comparing the raw and corrected DEMs. These analyses were conducted using QGIS version 3.34.9.

3.4. Flood-prone areas mapping using MCA—GT scale

MCA estimates flood susceptibility by combining various geospatial and climatic indicators, without explicitly modeling physical flow processes (Khosravi et al. 2019; Handini et al. 2021). This is particularly suited to data-poor contexts where hydrological simulations are constrained. The analysis includes the following nine indicators:

elevation, slope, Topographic Wetness Index (TWI), Stream Power Index (SPI), annual precipitation, land use, Normalized Difference Vegetation Index (NDVI), distance from rivers, and lithology (see Online Resource 1—Part 2 for further details). These variables were extracted from satellite imagery and open-source databases. Each indicator was subsequently normalized and classified into quantiles based on its influence on flood susceptibility.

All layers were integrated with equal weighting into a composite susceptibility index, using a Simple Additive Weighting (SAW) approach (Sar et al. 2025). Although several multicriteria analysis methods allow for differentiated weighting of criteria, either through distance-based or compromise-based calculations, or through structured expert judgment (Saaty 2013; Khosravi et al. 2019; Sar et al. 2025), applying such methods in this study would have introduced unjustifiable subjectivity due to the lack of validated regional data and local expertise (Decancq and Lugo 2013).

The resulting composite map was classified into quintiles—a standard method for mapping flood susceptibility (Khosravi et al. 2019) that distinguishes the following five categories: very low, low, moderate, high, and very high. Areas classified as 'very high' are the most vulnerable sectors, considered potentially prone to flooding.

All geospatial indicators were processed using SAGA GIS version 9.1.0 and QGIS version 3.34.9.

3.5. Validation and evaluation of flood impacts

The results were validated through comparison with field data collected during focus group discussions held in 2023 across 18 neighborhoods within the CUA. These neighborhoods were selected due to their high exposure to flooding and unfavorable conditions in terms of deprivation (Labatte et al. 2018; Ramiaramanana et al. 2025). Relying on their in-depth knowledge of the territory, local neighborhood agents identified and delineated the affected areas using location maps based on Google OpenStreetMap.

The assessment evaluated each approach's capability using key metrics, including sensitivity, specificity, accuracy, and negative predictive value. The results were cross-referenced with land use data to assess their impact in urban, peri-urban, and rural environments. Flood maps were also overlaid with residential building location data,

allowing for the quantification of affected infrastructure and the comparison of different methods in identifying impacted built-up areas.

The overall workflow integrating the three approaches is summarized in Fig. 2, and further technical details are available in Online Resource 1—Part 2.

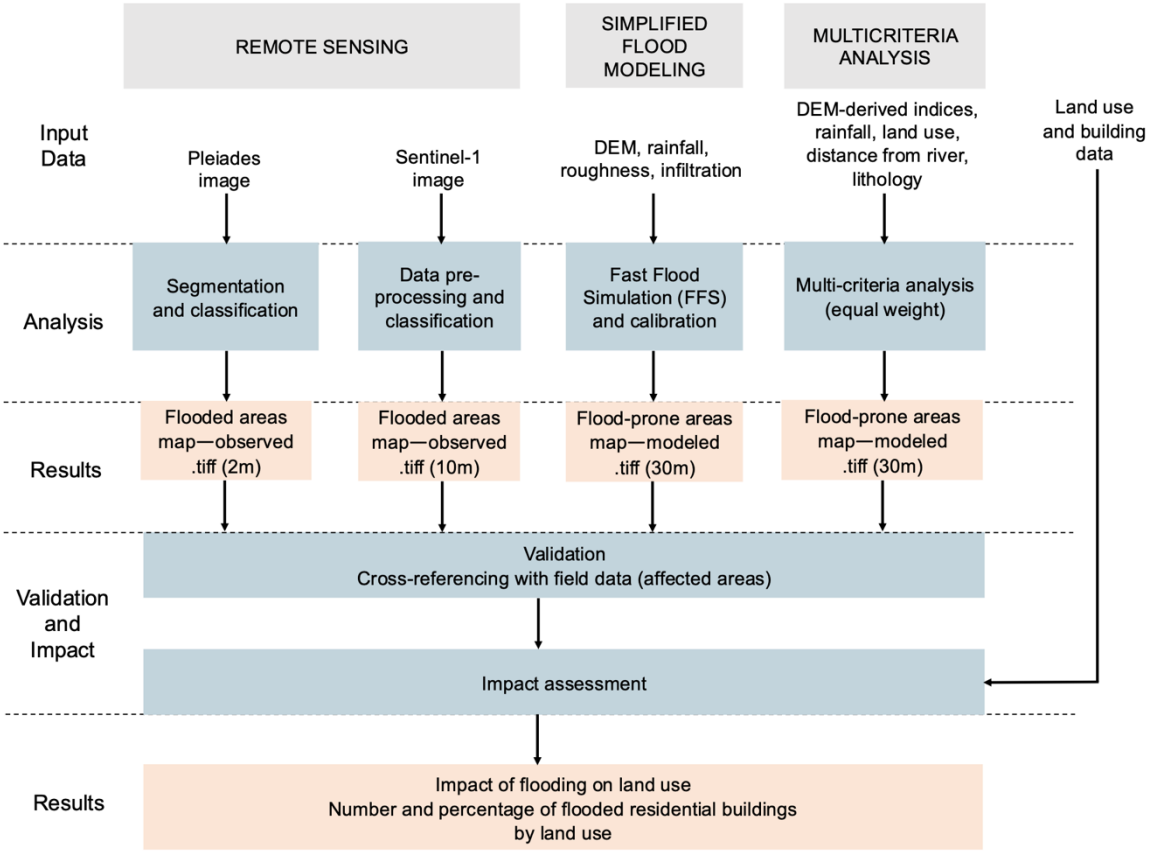

Fig. 2. Integrated workflow for flood mapping and impact assessment

4. Results

4.1. Flood mapping

4.1.1. Pleiades aerial imagery—CUA scale

The Pleiades image enabled detailed mapping of flooded areas in the CUA, primarily along river axes and topographical depressions. In the north of the study area, the convergence of multiple watercourses intensified water accumulation, while in the west, the low slope slowed drainage and prolonged flood stagnation (Fig. 3).

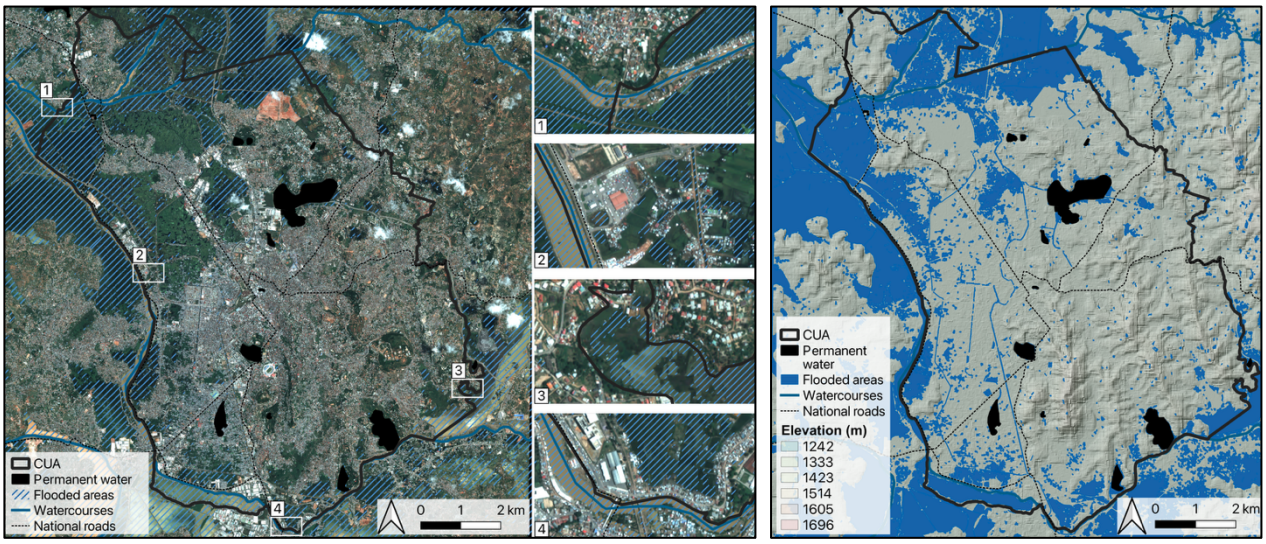

Fig. 3. Flooded areas based on Pleiades image (28/01/2022) displayed over the original optical image and a shaded topographic relief

Initial classification identified 17.41% of the area as flooded (**Erreur ! Source du renvoi introuvable.**). Manual corrections reduced this to 17.20% by addressing misclassifications caused by confusion with dark surfaces and unrecognized zones hidden by buildings (see Online Resource 1—Part 3).

Table 3. Distribution of flooded areas before and after correction, based on the Pleiades image

	Area	
Flooded areas	**ha**	**%**
Before correction	1,480	17.41
After correction	1,462.4	17.20
Difference	-17.6	-0.21

The analysis also highlighted the limitations of Pleiades imagery, which captures only surface-visible water, despite its high spatial resolution. Flooding under covered infrastructures or in densely vegetated areas thus escapes detection, leading to an underestimation of the surfaces affected, particularly in urban environments, where stagnant water can remain trapped under specific structures. Moreover, the data do not correspond to peak flooding, which limits the representativeness of the results and may potentially have led to a partial assessment of the actual extent of flooding.

4.1.2. Sentinel-1 radar imagery—GT scale

The Sentinel-1 radar imagery revealed localized flooding primarily along river corridors and in low-lying areas, especially in the western and southern peripheries of Antananarivo (Fig. 4). Only 3% of the CUA was identified as flooded, compared to 6.16% of the surrounding rural communes, indicating a more pronounced impact in outlying areas (**Erreur ! Source du renvoi introuvable.**).

Table 4. Distribution of flooded areas detected using the Sentinel-1 image

	Area	
Flooded areas	**ha**	**% (*)**
CUA	255.1	3
Peripheral communes	4,208.9	6.16
GT	4,464	5.80

(*) Percentages represent the flooded area of each zone as a proportion of its total area.

In urban environments, the density of infrastructure and reflective surfaces, such as buildings and roads, disrupt the radar signal, compromising flood detection. Some accumulations are visible in open areas, but the overall detection remains constrained by complex interactions with artificial infrastructure (Lin et al. 2019; Mason et al. 2023).

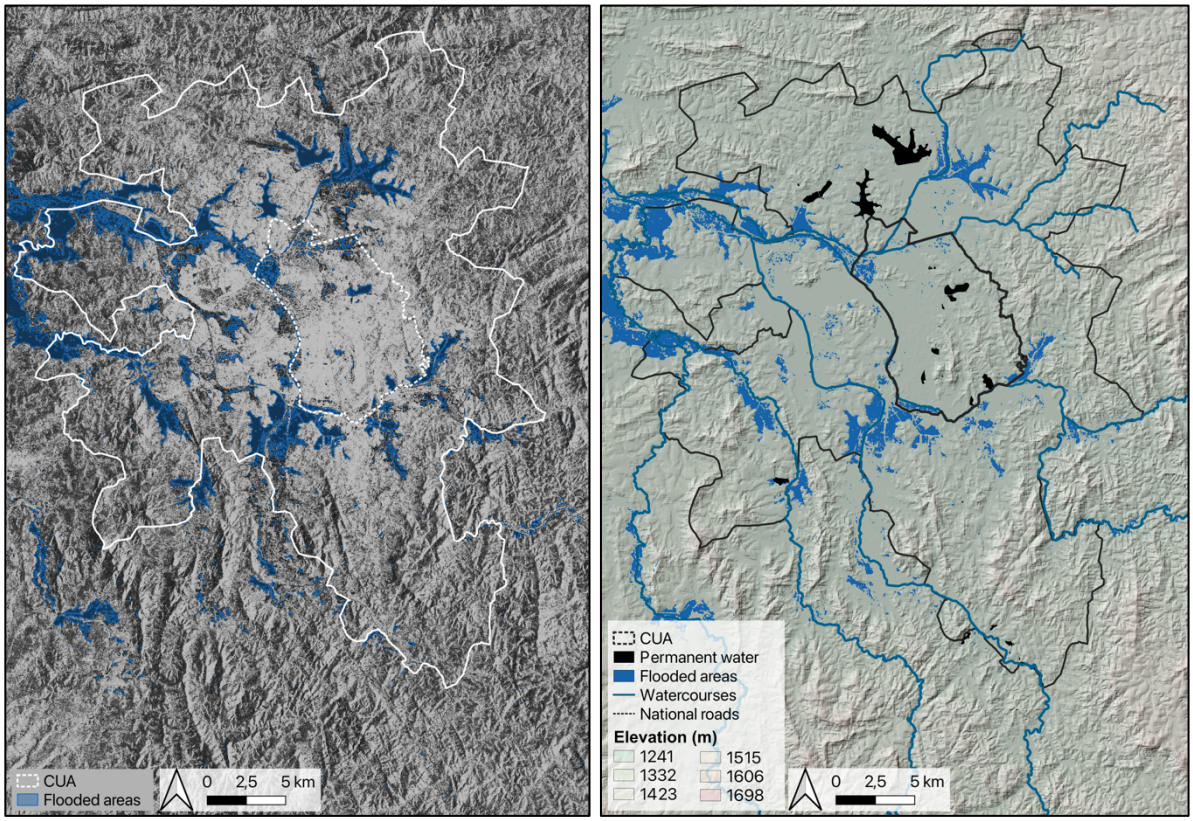

Fig. 4. Flooded areas extracted from the Sentinel-1 image (27/01/2022), displayed over the original radar image and a shaded topographic relief

4.1.3. Fast Flood Simulation model—GT scale

Unlike satellite-based methods, the FFS model estimated water depths and the extent of flooded areas by integrating field data and a specific hydrological event (Fig. 5). The simulations conducted across the study area showed that over 10% of flooded zones exceeded 2 m in depth, a critical threshold for safety and mobility in urban areas (see Online Resource 1—Part 4).

A comparison between the simulations using 10 cm and 25 cm depth thresholds showed a significant reduction in the flooded area within the CUA, with a decrease from 46.62% to 42.11% (Table 5; Fig. 5). This reflects the predominance of shallow flooding in urban environments. In peripheral areas, this decrease is more limited (from 31.44% to 28.47%), suggesting more persistent or deeper inundation (Table 5; Fig. 5). These differences highlight the sensitivity of the results to threshold selection.

Table 5. Distribution of flooded areas in 2022 based on various simulations

	Sim 1		Sim 2		Sim 3		Sim 4	
10 cm threshold	**ha**	**% (*)**	**ha**	**% (*)**	**ha**	**% (*)**	**ha**	**% (*)**
CUA	3,963.3	46.62	3,975.7	46.77	3,856.6	45.37	3,845.3	45.23
Peripheral communes	21,501	31.44	21,664.6	31.68	21,287.8	31.13	21,130.5	30.90
GT	25,464.2	33.12	25,640.3	33.35	25,144.3	32.70	24,975.9	32.49
25 cm threshold								
CUA	3,670.7	43.18	3,685.6	43.35	3,593.7	42.27	3,580.2	42.11
Peripheral communes	19,737.5	28.86	19,914.7	29.12	19,646.2	28.73	19,469.3	28.47
GT	23,408.2	30.45	23,600.3	30.70	23,239.9	30.23	23,049.5	29.98

(*) Percentages represent the flooded area of each zone as a proportion of its total area.

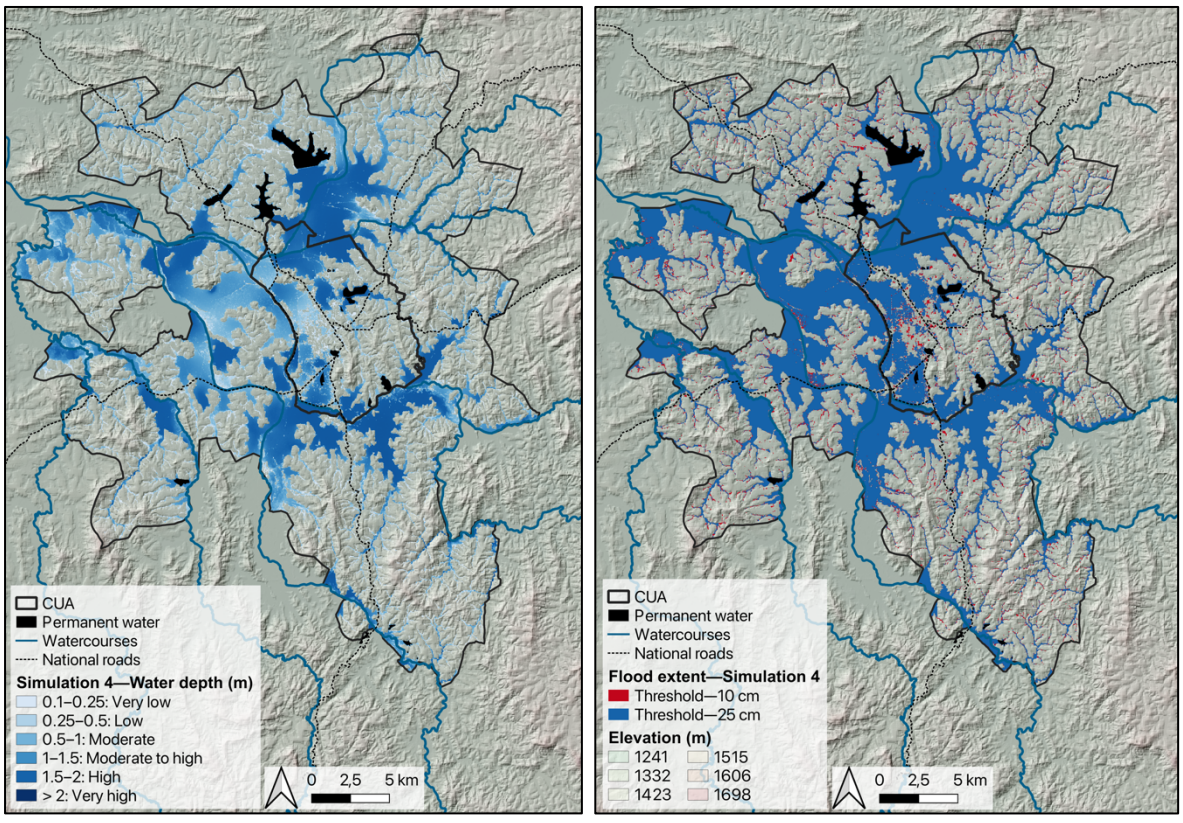

a. Water depths—24/01/2022

b. Flood extent with 10 cm and 25 cm thresholds

Fig. 5. Flooded areas—FFS—Simulation 4

Different parameter settings, particularly Manning's coefficient and infiltration, have a significant influence on flood behavior. Thus, the simulations using homogeneous roughness values (Simulations 1 and 2) produced a broader flood extent, while heterogeneous coefficients (Simulations 3 and 4) resulted in more localized water accumulations (Table 5). Infiltration demonstrated limited influence in urban areas due to high impermeability, but was found to contribute more noticeably to flood reduction in peripheral zones (Table 5; Online Resource 1—Part 4). These variations affected both the spatial extent and the depth distribution of floods, reinforcing the need for context-specific parameterization.

Adjustments to the DEM, particularly the correction of altimetric artifacts, significantly influenced the simulated water depth. Thus, riverbed slopes were reduced by up to 7.5°, and some artificially closed basins were opened, enhancing flow realism. These changes resulted in localized increases in the simulated depth, reaching up to +2.57 m in depressions and valley zones (see Online Resource 1—Part 4).

The cross-analysis by slope class revealed that in flat areas (0–2°), the corrected DEM redistributed flood volumes, increasing the proportion of zones with a depth exceeding 1 m. While this geometric correction improves hydraulic consistency by aligning accumulation with slope, caution is warranted. Specifically, when applied at a resolution of 30 m without field validation, this approach may artificially trap water and overestimate depths (see Online Resource 1—Part 4).

4.1.4. Multicriteria analysis—GT scale

The MCA mapped flood susceptibility by classifying the territory into five levels of vulnerability based on environmental and geospatial criteria divided into quintiles. Unlike the Sentinel-1, Pleiades, and FFS approaches, which detect actual flooding, this method identifies areas structurally that are exposed to risk independently of temporary hydrological conditions.

The results show that 60% of the CUA is classified as exhibiting 'high' or 'very high' susceptibility, including 39.56% of the area being classified within the highest category (Table 6**Erreur ! Source du renvoi introuvable.**). This reflects the low elevation, flat slopes, high imperviousness, and topographic indices in urban zones that favor water accumulation (Fig. 6).

In the peripheral communes, the risk distribution is more balanced; however, about 20% remains in the 'very high' susceptibility class. These areas are mainly located along watercourses with compact soils, limited vegetation cover, and a low infiltration capacity (Table 6**Erreur ! Source du renvoi introuvable.**; Fig. 6). Overall, 22.19% of the agglomeration falls within the highest vulnerability class, underlining systemic vulnerability linked to urban expansion and watershed constraints (Table 6**Erreur ! Source du renvoi introuvable.**). Notably, although this approach is based on a rigorous multicriteria assessment, this method does not incorporate hydrodynamics or upstream–downstream interactions. As a result, flood exposure may be over- or underestimated in some areas, limiting its predictive reliability in isolation.

Table 6. Distribution of areas by flooding susceptibility class

	Area									
Susceptibility class	**Very low**		**Low**		**Moderate**		**High**		**Very high**	
	ha	**% (*)**	**ha**	**% (*)**	**ha**	**% (*)**	**ha**	**% (*)**	**ha**	**% (*)**
CUA	267.6	3.21	961	11.55	1,590.9	19.11	2,209.8	26.55	3,291.6	**39.56**
Peripheral communes	13,460.4	19.98	14,355.1	21.31	13,286.5	19.72	12,771.1	18.95	13,503.9	**20.04**
GT	13,728	18.13	15,316.2	20.23	14,877.4	19.65	14,980.9	19.79	16,795.5	**22.19**

(*) Percentages indicate the area of each zone that falls within each susceptibility class as a proportion of the total area of the corresponding zone.

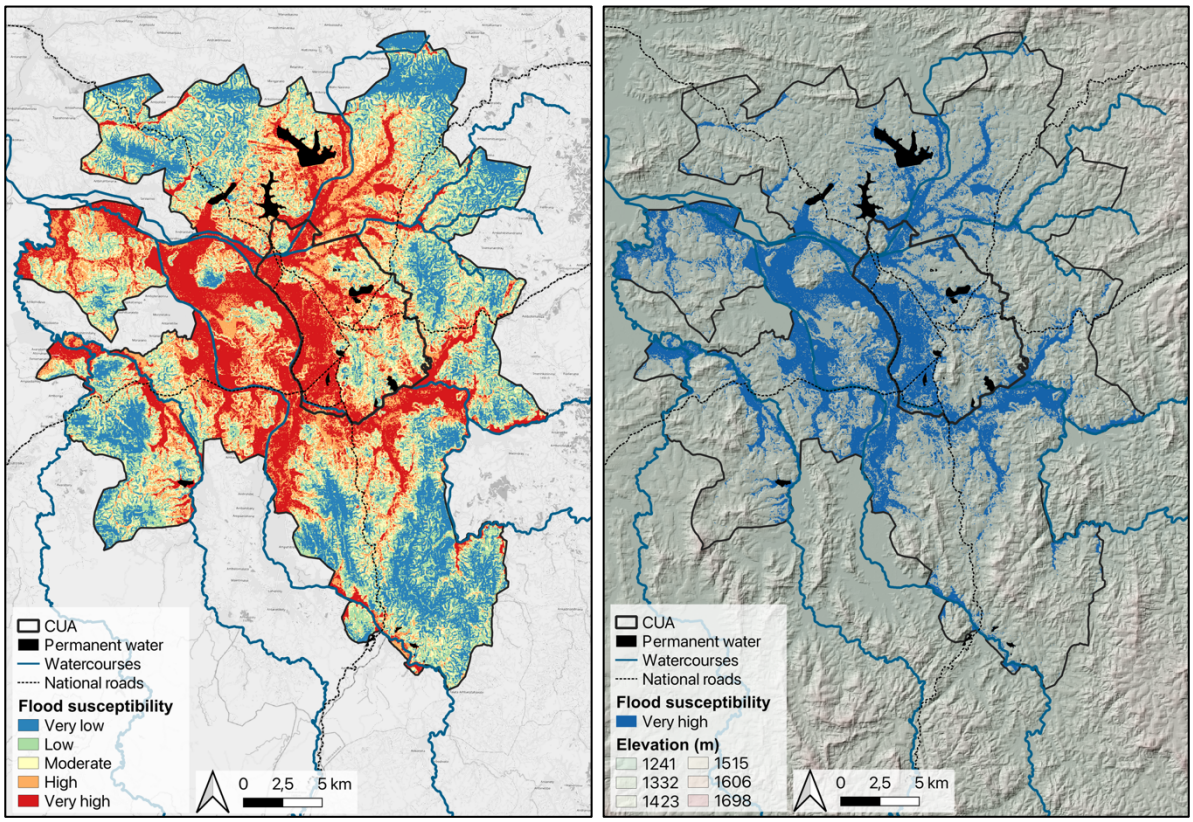

a. Flood susceptibility levels b. Very high level of flood susceptibility

Fig. 6. Flood susceptibility levels—MCA

4.2. Validation

Validation of the results was conducted using field data from 18 neighborhoods; full details are provided in Online Resource 1—Part 6. The satellite-based methods (Pleiades and Sentinel-1) showed high specificity (97.7% and 99.8%, respectively), indicating a strong ability to exclude non-flooded areas. However, their sensitivity remained low, at 15.12% for Pleiades and just 0.32% for Sentinel-1, leading to considerable underestimation of flooded surfaces. This underperformance is primarily due to differences in spatial resolution and sensor type: the high-resolution optical imagery from Pleiades enables better detection of small and localized flood events compared to Sentinel-1. However, both sensors face limitations in urban environments, where vegetation, buildings, and infrastructure can obscure surface water. Radar signals from Sentinel-1 are particularly disrupted in dense areas, and optical imagery may not capture water trapped beneath structures. This restrictive approach, typically used in data-poor environments, limits the ability to identify vulnerable areas and implement appropriate measures. In the context of climate change, where extreme events are expected to intensify, these methods seem ill suited to anticipate the evolution of risks.

The FFS simulations performed consistently better. With a 10 cm threshold, the sensitivity ranged from 77.31% to 79.53%, and the specificity reached above 92%, providing a more reliable spatial delineation of flood extent. With a 25 cm threshold, the sensitivity decreased slightly but the specificity improved (up to 93%), which would reduce false alarms and preventing the misallocation of resources and the imposition of unnecessary restrictions on urban planning. Integrating spatial variability into the Manning coefficients and infiltration (Sim 4) enhanced the model's accuracy by reducing underestimation and improving reliability, an essential advantage in data-scarce environments.

The MCA approach yielded intermediate results, with a sensitivity of 68.15%, a specificity of 94.41%, and higher precision (44.67%) compared to the satellite-based methods. Thus, despite its coarser spatial resolution, MCA offers a pragmatic trade-off, minimizing false positives while moderately underestimating flood extent.

These results underscore the importance of selecting the appropriate methodology to address operational requirements. When omission errors pose critical risks, such as underestimating flooding that threatens populations or infrastructure, FFS-Sim4 (10 cm) offers the best balance between sensitivity and reliability. MCA is also better suited when classification stability and the reduction of false positives are priorities, which particularly tends to be the case in land use planning. Nevertheless, satellite methods, such as Sentinel-1 and Pleiades, lack the sensitivity required for flood detection, especially in urban contexts, they remain valuable for validation and post-event monitoring. A combined approach is thus recommended to strengthen the capacity for early warning and adaptation planning, particularly in data-scarce settings that are exposed to increasing flood risks under climate change.

4.3. Impact assessment

4.3.1. Impact based on land use

The analysis reveals significant disparities in flood assessment based on land use and the different tools employed (see Online Resource 1—Part 7 for further details). Agricultural and wetland areas appear to be particularly vulnerable due to low infiltration and poor drainage. By using FFS at the 10 cm threshold, 83.55% of flooded agricultural land was detected within the CUA, and 59.45% was detected in peripheral communes. These values decreased slightly at the 25 cm threshold (81.42% and

55.49%), indicating the dominance of shallow flooding in these areas. MCA significantly underestimated flood extents in agricultural zones (56.41% in peripheral communes and 32.19% in the CUA), a limitation that may compromise planning and adaptation strategies.

Sentinel-1, although limited in urban and vegetated environments, captured more flood signals in open peri-urban areas (12.03% of agricultural land on the outskirts). Although Pleiades imagery offers higher spatial resolution, its limited coverage reduces its effectiveness in assessing complex phenomena such as water infiltration and accumulation. In data-scarce environments, this underestimation may hinder preventive action by limiting the detection of large-scale accumulation patterns.

In residential areas, impervious surfaces influence flood distribution. FFS detected 19.87% of flooded residential land in the CUA (10 cm threshold), and this value decreased to 16.60% at the 25 cm threshold, reflecting the importance of surface flooding. MCA detected higher proportions (28.62%), which may reflect overestimation due to the model's generalized runoff assumptions; this may potentially lead to inefficient resource mobilization by directing interventions towards areas where the risk is exaggerated. Pleiades captured less than 1% of the flooding, likely due to the complexity of dense urban environments, whereby the interactions between infiltration, runoff, and drainage complicate flood detection and monitoring.

The results obtained when increasing the FFS threshold from 10 cm to 25 cm illustrate differences in flood depth across land use types. For example, in the CUA, the most notable reductions occurred in residential areas (–3.27%) and industrial regions (–7.28%), which is consistent with surface-level flooding. In the peripheral agricultural zones, the reduction was more moderate (–3.96%), yet the persistence of water depths above 25 cm underscores a higher vulnerability to erosion, agricultural loss, and ecosystem disturbance (see Online Resource 1—Part 7).

While urban flooding is often shallow, its recurrent nature significantly affects mobility and infrastructure. The resulting impacts therefore depend on surface permeability and the performance of the drainage system. Industrial zones, though less frequently affected, require detailed risk assessment to ensure business continuity. Overall, flood mitigation strategies should be tailored to local land use conditions, combining appropriate infrastructure with the preservation of natural buffers.

4.3.2. Impact on residential buildings

The assessment of flood exposure in residential areas revealed that FFS and MCA detected the highest proportions of affected buildings in the CUA, at 27.65% (FFS at 10 cm) and 37.03% (MCA), compared to 10.26% and 17.62%, respectively, in the peripheral areas (Fig. 7).

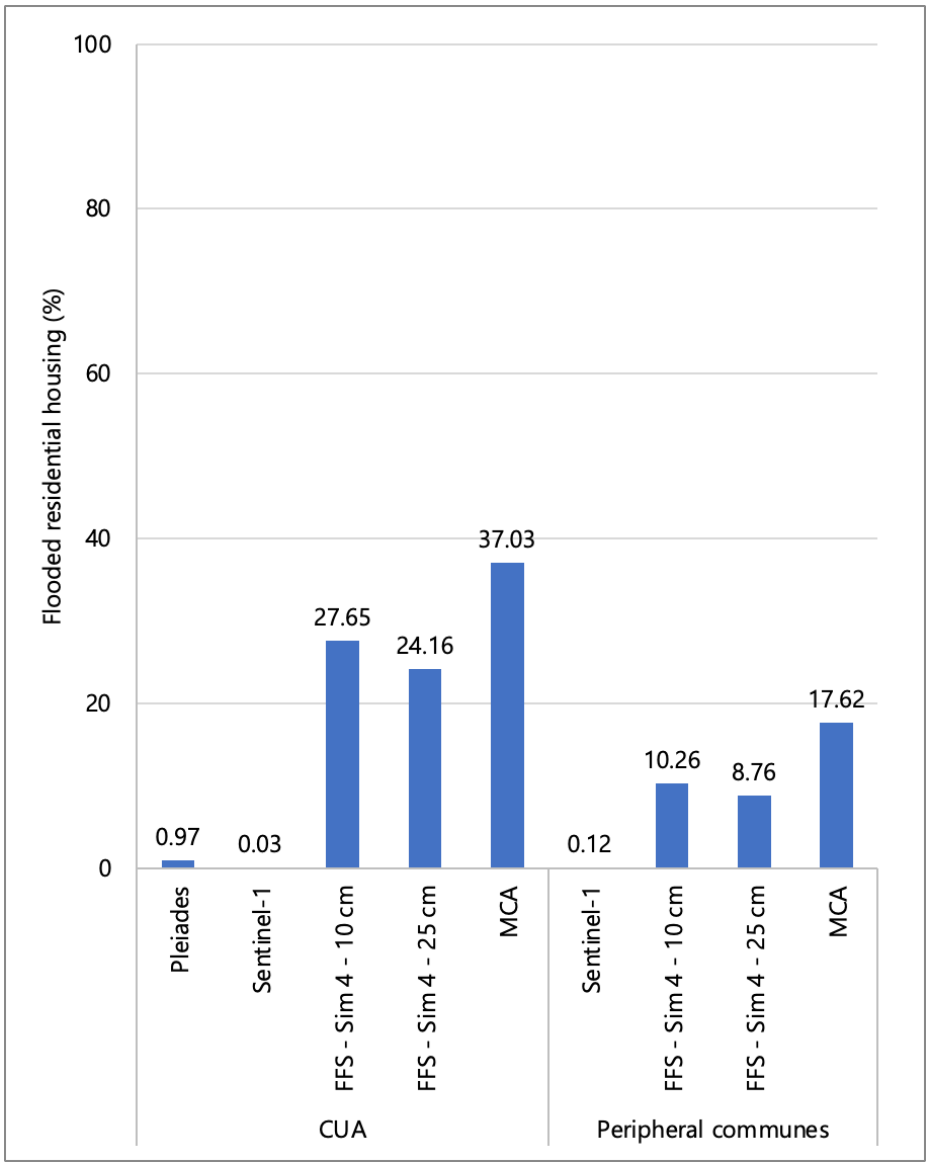

Fig. 7. Distribution of flooded residential buildings detected using each flood mapping tool

The reduction observed using FFS at the 25 cm threshold (24.16% in the CUA and 8.76% in the peripheral areas) emphasizes that flooding remains a concern in built-up areas.

MCA may overestimate impacts due to its limited ability to account for local drainage, while FFS, though more sensitive to runoff, may underestimate flooding in densely built areas with altered hydrological dynamics. Conversely, Sentinel-1 and Pleiades detected very few flooded buildings, especially in the CUA (0.03% and 0.97%, respectively), due to radar limitations and restricted spatial coverage (Fig. 7).

An in-depth analysis of the CUA revealed that FFS and MCA identified the majority of flooded buildings in residential areas, with detection rates of 22.39% at the 10 cm threshold and 19.46% at the 25 cm threshold, and 31.81%, respectively (Online Resource 1—Part 7). This concentration aligns with high impervious surface coverage, which promotes water retention even at greater depths (25 cm), thereby increasing structural vulnerability and disrupting local socio-economic activity. Sentinel-1 detected only eight affected residential buildings, confirming its tendency for underestimation in dense urban areas.

Outside of the residential areas, FFS and MCA identified buildings in wetlands (2.02% at the 10 cm threshold and 1.90% at the 25 cm threshold, and 1.35%, respectively), indicating a more accurate representation of flooding in urban areas. Pleiades performed modestly better than Sentinel-1 in these areas (0.20% vs. near zero), thanks to its higher spatial resolution, which improves its ability to detect isolated structures. The residential buildings in these wetlands reveal the heightened risks associated with precarious or unregulated housing; frequently excluded from traditional flood management strategies, these structures remain at risk due to inadequate drainage infrastructure and access to warning systems. This highlights the need for enhanced integration of these areas into preventive policies.

5. Discussion

5.1. Performance and reliability of the different methods

The FFS model stands out for its ability to estimate water depth, a crucial parameter for assessing the vulnerability of exposed assets. This quantitative dimension enhances traditional flood mapping by supporting the identification of critical thresholds and informing adaptation strategies. Its performance, however, depends on careful calibration and the quality of input data, particularly for precipitation and the DEM (Massari et al. 2014; Glas 2023; Watson et al. 2024). In flat or densely urbanized areas, slope adjustments may generate artificial accumulations and distort risk estimations without ground validation. Moreover, the absence of explicit representation of

infrastructure and drainage systems in FFS can result in significant over- or underestimation in complex urban settings, where the performance of the model may vary across geographical contexts (Ketu 2024; Munyi 2024). The model also requires hydrological expertise (Glas 2023), as misconfigured parameters or misinterpretation of outputs can compromise the reliability of the results and the effectiveness of decision-making.

Remote sensing tools provide complementary observations. Sentinel-1 performs well in rural or open areas (Mason et al., 2023), whereas Pleiades offers high spatial resolution for detailed mapping (Huber et al. 2013; Maxant et al. 2013; Mason et al. 2023). However, both are constrained in urban contexts; radar signals are affected by building interference, and optical sensors may fail to capture inundation beneath dense structures or under cloud cover (Yésou et al. 2015; Qiu et al. 2021; de Liz and Ribas 2022; Tanim et al. 2022). Acquisition timing further limits their reliability during short-duration flood peaks (Notti et al. 2018; Tarpanelli et al. 2022). These factors explain the lower sensitivity observed in the results, leading to missed detections that can underestimate exposed populations and delay emergency interventions. Occasional misclassifications may also trigger false positives, diverting limited resources to unaffected areas. Additionally, the high cost and restricted accessibility of commercial imagery, such as Pleiades imagery, limit its large-scale application in low-resource settings (IGN 2018; Mukhopadhyay et al. 2024).

MCA offers a flexible framework for prioritizing flood-prone areas, particularly for long-term planning; however, its reliability depends on the weighting of the indicators (Dodgson et al. 2009; Khosravi et al. 2019; Akindele and Todome 2021). In urban environments, the heterogeneity of exposure may compromise spatial accuracy, potentially leading to inefficient allocation of resources if calibration is inadequate.

Table 7 provides an overview of these approaches' main features, advantages, and limitations of the different approaches assessed in this study.

Table 7. Characteristics, advantages, and limitations of each approach assessed in this study

Tool	Data accessibility	Key benefits	Optimal applications	Specific limitations
FFS	Open access	- Rapid flood detection - Water depth estimation - Simulates multiple events	- Scenario modeling - Crisis response	- Sensitive to input data quality and calibration parameters - Variable urban performance - May trigger false alarms
MCA	Open access	- Event-independent - Detailed risk mapping - Supports spatial planning	- Vulnerability assessment - Long-term planning	- Does not simulate events - May overestimate urban exposure
Sentinel-1	Open access	- Operates under cloud cover - Effective in rural/low-density areas	- Flood dynamics validation	- Affected by urban reflectivity - Limited surface flood detection
Pleiades	Restricted access (licensed data)	- Very high resolution - Fine-scale surface flood detection	- Urban and peri-urban analysis	- Requires field validation - Weather-sensitive - Urban masking - May miss shallow/short floods

5.2. Complementarity of tools in the flood management decision-making process

The complementarity of the tools analyzed in this study supports their integration into a structured, multi-phase flood management framework. As shown in Fig. 8, their interaction optimizes strategic planning and operational response capabilities. In the prevention phase, FFS can anticipate risk by simulating flood scenarios, helping to identify priority areas for intervention (Glas 2023). However, in urban contexts, its

accuracy may be limited by the absence of explicit infrastructure representation, which affects the dynamics of runoff. Remote sensing, via Sentinel-1 and Pleiades, can complement FFS by providing spatial validation and refining local-scale analysis. These datasets can aid in detecting anomalies and validating model output when model assumptions are constrained (Nguyen et al. 2021; de Liz and Ribas 2022). MCA adds a decision-support layer by structuring complex, multi-criteria information (Papaioannou et al. 2015); it enables prioritization and investment planning tailored to territorial characteristics, especially for long-term flood risk management.

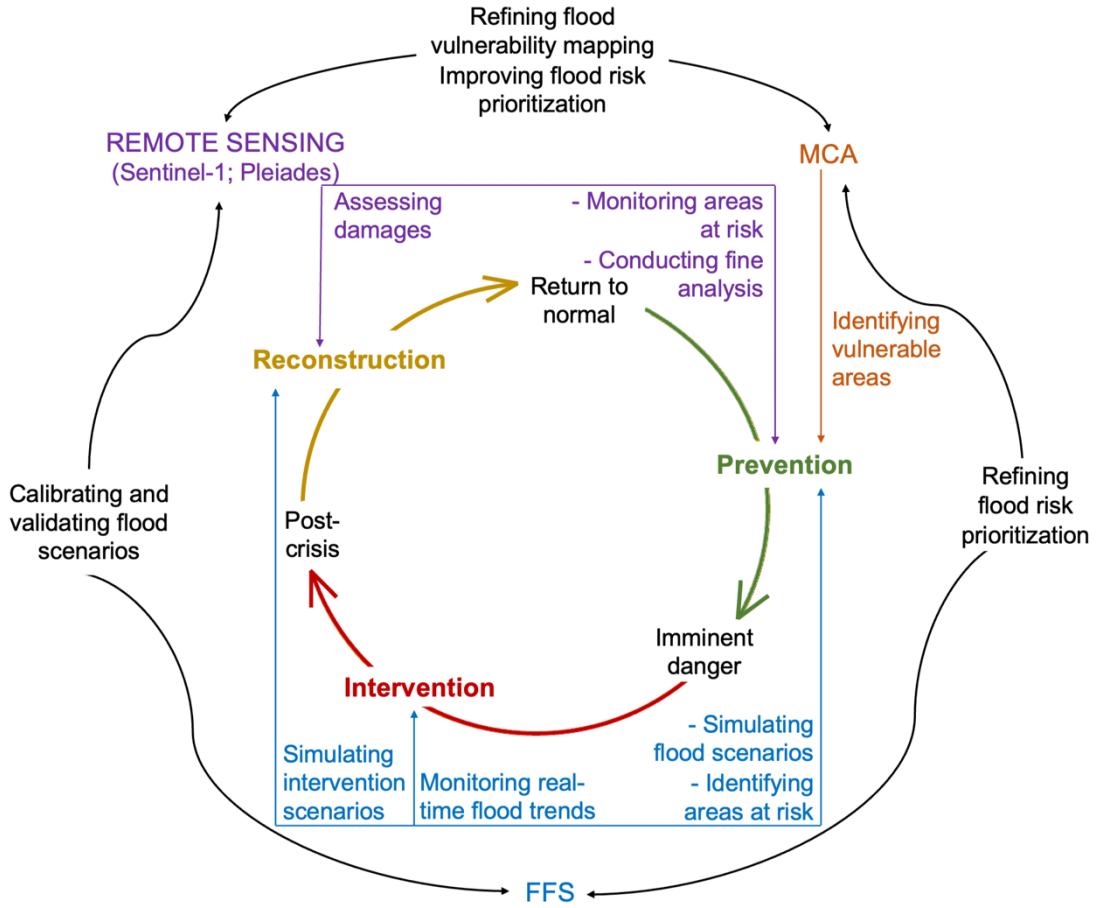

Fig. 8. The functional integration and complementarity of tools in the flood management decision-making process

During the response phase, FFS remains a key tool for real-time scenario updates, enabling the rapid adjustment of emergency strategies (Van den Bout et al. 2023). Its fast computational performance can support dynamic coordination during crises. In the reconstruction phase, integrating FFS with satellite imagery can enable impact mapping and support scenario-based planning. Sentinel-1 and Pleiades can assist in

identifying damaged infrastructure and quantifying losses (Yésou et al. 2015; Uddin et al. 2019; Sadiq et al. 2023), while FFS simulations can guide resilient reconstruction and model recalibration using post-event data.

These tools can be integrated into a unified decision-support system, such as a GIS platform or dashboard, where each tool provides a complementary layer of information; FFS offers predictive simulations, remote sensing delivers observed impacts, and MCA supports prioritization. Their outputs can converge into a single interface, allowing stakeholders to interpret risks coherently across scales and phases. This integration ensures that decisions—whether preventive, responsive, or recovery-oriented—are based on a shared, spatially explicit, and evidence-driven foundation, strengthening coordination and resource targeting, particularly in data-scarce environments.

5.3. Strategic implications and outlook

The large-scale integration of these tools requires appropriate institutional and technical structuring, particularly in data-poor environments, where the ability of the tools to operate with limited information makes them particularly valuable. Local capacity-building is crucial for ensuring the optimal use of these tools. User training and methodology standardization will further promote greater interoperability and reliability of analyses. A collaborative approach involving researchers, institutions, and local stakeholders is essential if these tools are to be incorporated into risk management policies adapted to data-limited contexts, thereby strengthening resilience to flooding.

5.4. Study limitations

This study had two main limitations. First, it did not incorporate the spatio-temporal variability of hydrological processes, which constrained the analysis of flood dynamics across different time scales. Second, the FFS model was applied to a single high-intensity rainfall event, selected for its relevance and data availability. While this scenario provides meaningful insight, a multi-scenario approach would have improved model robustness and broadened our understanding of flood behavior under diverse conditions (Glas 2023).

6. Conclusion

This study highlights the respective strengths and limitations of several flood mapping tools, which were applied in Antananarivo, Madagascar. The FFS model supports vulnerability assessment and water level estimation but relies heavily on the quality of the DEM and the accuracy of model calibration. Sentinel-1 offers all-weather flood detection yet struggles in urban settings due to infrastructure interference, and while Pleiades provides high-resolution flood mapping, its effectiveness is limited by access restrictions, urban shadowing, weather sensitivity, and the need for complementary field validation. MCA facilitates strategic prioritization, but it must be coupled with dynamic modeling to be operationally effective.

Integrating these tools has the potential to enhance flood analysis in data-scarce environments by offsetting individual limitations. In prevention, FFS and satellite data can improve planning, while MCA can guide resource allocation. During crises, FFS can support real-time strategy adjustment. In recovery, FFS combined with remote sensing can enable accurate damage assessment and inform resilient reconstruction.

Optimizing these tools requires improved data interoperability, coordinated calibration protocols, and the integration of urban infrastructure into models. It is equally crucial to strengthen local capacity through targeted training and context-specific early-warning systems, to ensure more effective and adaptive flood risk management.

References

Abunyewah M, Gajendran T, Maund K (2018) Profiling Informal Settlements for Disaster Risks. Procedia Eng 212:238–245. https://doi.org/10.1016/j.proeng.2018.01.031

Akindele AA, Todome L (2021) Flood risk assessment by a multicriteria spatial analysis in the municipalities of Pobè and Adja-Ouèrè. Int J Engl Lit Soc Sci 6:120–129. https://doi.org/10.22161/ijels.63.20

Amitrano D, Di Martino G, Iodice A, et al (2018) Unsupervised rapid flood mapping using Sentinel-1 GRD SAR images. IEEE Trans Geosci Remote Sens 56:3290–3299. https://doi.org/10.1109/TGRS.2018.2797536

Anusha N, Bharathi B (2020) Flood detection and flood mapping using multi-temporal synthetic aperture radar and optical data. Egypt J Remote Sens Space Sci 23:207–219. https://doi.org/10.1016/j.ejrs.2019.01.001

Anwana EO, Owojori OM (2023) Analysis of flooding vulnerability in informal settlements literature: mapping and research agenda. Soc Sci 12:40. https://doi.org/10.3390/socsci12010040

Arnell NW, Gosling SN (2016) The impacts of climate change on river flood risk at the global scale. Climatic Change 134:387–401. https://doi.org/10.1007/s10584-014-1084-5

Arnold JG, Fohrer N (2005) SWAT2000: current capabilities and research opportunities in applied watershed modelling. Hydrol Process 19:563–572. https://doi.org/10.1002/hyp.5611

ARTELIA (2014) Elaboration du schéma directeur d'Assainissement Urbain du Grand Tana. Rapport technique. Antananarivo, Madagascar

Attoumani A, Victor R, Randriamampandry C, Andrianirina R (2019) La croissance de la ville d'Antananarivo et ses conséquences. Madamines 1:1–25

Baker JL (2012) Climate change, disaster risk, and the urban poor: cities building resilience for a changing world. World Bank, Washington, DC

Beshir AA, Song J (2021) Urbanization and its impact on flood hazard: the case of Addis Ababa, Ethiopia. Nat Hazards 109:1167–1190. https://doi.org/10.1007/s11069-021-04873-9

Bhatt CM, Rao GS, Jangam S (2020) Detection of urban flood inundation using RISAT-1 SAR images: A case study of Srinagar, Jammu and Kashmir (North India) floods of September 2014. Model Earth Syst Environ 6:429–438. https://doi.org/10.1007/s40808-019-00690-z

Blaschke T (2010) Object-based image analysis for remote sensing. ISPRS J Photogramm Remote Sens 65:2–16. https://doi.org/10.1016/j.isprsjprs.2009.06.004

Brunner GW (1997) HEC-RAS river analysis system. Hydraulic reference manual. Version 1.0. Hydrologic Engineering Center, US Army Corps of Engineers, Davis, CA

Chen Y, Zhou H, Zhang H, et al (2015) Urban flood risk warning under rapid urbanization. Environ Res 139:3–10. https://doi.org/10.1016/j.envres.2015.02.028

Chen Y-R, Yeh C-H, Yu B (2011) Integrated application of the analytic hierarchy process and the geographic information system for flood risk assessment and flood plain management in Taiwan. Nat Hazards 59:1261–1276. https://doi.org/10.1007/s11069-011-9831-7

Ciampalini A, Frodella W, Margottini C, Casagli N (2019) Rapid assessment of geo-hydrological hazards in Antananarivo (Madagascar) historical centre for damage prevention. Geom Nat Haz Risk

10:1102–1124. https://doi.org/10.1080/19475705.2018.1564375
Cohen B (2006) Urbanization in developing countries: Current trends, future projections, and key challenges for sustainability. Technol Soc 28:63–80. https://doi.org/10.1016/j.techsoc.2005.10.005
CRED (2024) 2023 Disasters in numbers - World | ReliefWeb. https://reliefweb.int/report/world/2023-disasters-numbers. Accessed 5 Jun 2024
Dao PD, Mong NT, Chan H-P (2019) Landsat-MODIS image fusion and object-based image analysis for observing flood inundation in a heterogeneous vegetated scene. GISci Remote Sens 56:1148–1169. https://doi.org/10.1080/15481603.2019.1627062
de Liz MSM, Ribas RP (2022) Flood extent delineation using Sentinel-1 data as information source: systematic review of processing methods. Revista Brasileira de Geografia Física 15:3047–3076
Decancq K, Lugo MA (2013) Weights in Multidimensional Indices of Wellbeing: An Overview. Econometric Reviews 32:7–34. https://doi.org/10.1080/07474938.2012.690641
Defrise L, Burnod P, Andriamanga V (2017) Terres agricoles de la ville d'Antananarivo, une disparition inéluctable? Université d'Antananarivo, Antananarivo
Denis A (2019) Adapted transcription of ESA Echoes in Space-Hazard: Flood mapping with Sentinel-1 tutorial (ESA EO College)
Devi GK, Ganasri BP, Dwarakish GS (2015) A review on hydrological models. Aquatic Procedia 4:1001–1007. https://doi.org/10.1016/j.aqpro.2015.02.126
Diop A, Ndiaye ML, Sambou H, et al (2017) Integrated a GIS and multicriteria evaluation approach for mapping flood vulnerability of buildings in the Grande Niaye Watershed of Dakar, Senegal. American Journal of Geographic Information System 6:41–53. https://doi.org/10.5923/j.ajgis.20170602.01
Dodgson JS, Spackman M, Pearman A, Phillips LD (2009) Multi-criteria analysis: a manual. Department for Communities and Local Government, London
Doocy S, Daniels A, Murray S, Kirsch TD (2013) The human impact of floods: a historical review of events 1980-2009 and systematic literature review. PLoS Curr 5:. https://doi.org/10.1371/currents.dis.f4deb457904936b07c09daa98ee8171a
Douglas I, Alam K, Maghenda M, et al (2008) Unjust waters: climate change, flooding and the urban poor in Africa. Environment and Urbanization 20:187–205. https://doi.org/10.1177/095624780808915
Dupuy S, Andriamanga AV, Burnod P (2023) Antananarivo–Madagascar–land use change map between 2017 and 2022. CIRAD Dataverse. https://doi.org/10.18167/DVN1/CD2ZTF
Fatti CE, Patel Z (2013) Perceptions and responses to urban flood risk: implications for climate governance in the South. Appl Geogr 36:13–22. https://doi.org/10.1016/j.apgeog.2012.06.011
Gashaw W, Legesse D (2011) Flood hazard and risk assessment using GIS and remote sensing in Fogera Woreda, Northwest Ethiopia. In: Melesse AM (ed) Nile River Basin. Springer Netherlands, Dordrecht, pp 179–206
Glas V (2023) Application of the fast flood simulation model for local risk-informed decision-making on flood risk reduction: a case study of Pamba Basin, Kerala India. Master's Thesis, University of Twente
Handini DR, Hidayah E, Halik G (2021) Flash flood susceptibility mapping at Andungbiru watershed,

East Java using AHP-information weighted method. Geosfera Indonesia 6:127–142. https://doi.org/10.19184/geosi.v6i2.24173
Herrero AD, Huerta LL, Isidro ML (2009) A handbook on flood hazard mapping methodologies. Geological Survey of Spain, Madrid
Hirabayashi Y, Mahendran R, Koirala S, et al (2013) Global flood risk under climate change. Nat Clim Chang 3:816–821. https://doi.org/10.1038/nclimate1911
Huber C, Battiston S, Yésou H, et al (2013) Synergy of VHR pleiades data and SWIR spectral bands for flood detection and impact assessment in urban areas: Case of Krymsk, Russian Federation, in July 2012. In: IEEE International Geoscience and Remote Sensing Symposium-IGARSS. IEEE, pp 4538–4541
Hunter NM, Bates PD, Horritt MS, Wilson MD (2007) Simple spatially-distributed models for predicting flood inundation: A review. Geomorphology 90:208–225. https://doi.org/10.1016/j.geomorph.2006.10.021
IGN (2018) Guide utilisateur Pléiades : offre de produits et services
Jaber FH, Shukla S (2012) MIKE SHE: Model use, calibration, and validation. Transactions of the ASABE 55:1479–1489. https://doi.org/10.13031/2013.42255
Janicka E, Kanclerz J (2022) Assessing the effects of urbanization on water flow and flood events using the HEC-HMS model in the Wirynka River Catchment, Poland. Water 15:86. https://doi.org/10.3390/w15010086
Janizadeh S, Pal SC, Saha A, et al (2021) Mapping the spatial and temporal variability of flood hazard affected by climate and land-use changes in the future. J Environ Manage 298:113551. https://doi.org/10.1016/j.jenvman.2021.113551
Kakinuma K, Puma MJ, Hirabayashi Y, et al (2020) Flood-induced population displacements in the world. Environ Res Lett 15:124029. https://doi.org/10.1088/1748-9326/abc586
Ketu JA (2024) Assessing the impact of future rainfall and urban growth on flood hazard in Kumasi, Ghana: Identifying potential flood mitigation measures. Master's Thesis, University of Twente
Khosravi K, Shahabi H, Pham BT, et al (2019) A comparative assessment of flood susceptibility modeling using multi-criteria decision-making analysis and machine learning methods. J Hydrol 573:311–323. https://doi.org/10.1016/j.jhydrol.2019.03.073
Kumar V, Sharma KV, Caloiero T, et al (2023) Comprehensive overview of flood modeling approaches: A review of recent advances. Hydrology 10:141. https://doi.org/10.3390/hydrology10070141
Labatte B, Mazoyer A, Recouvreur R, et al (2018) PIAA : Diagnostic qualificatif et sectorisation thématique - Fascicule 6 : thématique des eaux pluviales. BRL Ingénierie, Antananarivo
Lambert M, Recouvreur R, Marty D, Janssen J (2017) Mission de maîtrise d'oeuvre pour le Programme Intégré d'Assainissement d'Antananarivo (PIAA). BRL Ingénierie
Li J, Zhou W, Tao C (2024) The impact of urbanization on surface runoff and flood prevention strategies: a case study of a traditional village. Land 13:1528. https://doi.org/10.3390/land13091528
Li W, Lin K, Zhao T, et al (2019) Risk assessment and sensitivity analysis of flash floods in ungauged basins using coupled hydrologic and hydrodynamic models. J Hydrol 572:108–120. https://doi.org/10.1016/j.jhydrol.2019.03.002

Lin L, Di L, Yu EG, et al (2016) A review of remote sensing in flood assessment. In: 2016 Fifth International Conference on Agro-Geoinformatics (Agro-Geoinformatics). IEEE, pp 1–4
Lin YN, Yun S-H, Bhardwaj A, Hill EM (2019) Urban flood detection with Sentinel-1 multi-temporal synthetic aperture radar (SAR) observations in a Bayesian framework: a case study for Hurricane Matthew. Remote Sens 11:1778. https://doi.org/10.3390/rs11151778
Liuzzo L, Sammartano V, Freni G (2019) Comparison between different distributed methods for flood susceptibility mapping. Water Resour Manage 33:3155–3173. https://doi.org/10.1007/s11269-019-02293-w
Mason DC, Dance SL, Cloke HL (2023) Toward improved urban flood detection using Sentinel-1: dependence of the ratio of post-to preflood double scattering cross sections on building orientation. J Appl Remote Sens 17:016507–016507. https://doi.org/10.1117/1.JRS.17.016507
Massari C, Brocca L, Moramarco T, et al (2014) Potential of soil moisture observations in flood modelling: estimating initial conditions and correcting rainfall. Adv Water Resour 74:44–53. https://doi.org/10.1016/j.advwatres.2014.08.004
Maxant J, Proy C, Fontannaz D, et al (2013) Contribution of Pléiades-HR imagery for disaster damage mapping: initial feedback over Asia, Africa, Europe or the Caribbean. In: Proceedings of 33th EARSeL Symposium Towards Horizon. p 8
McCormack T, Campanyà J, Naughton O (2022) A methodology for mapping annual flood extent using multi-temporal Sentinel-1 imagery. Remote Sens Environ 282:113273. https://doi.org/10.1016/j.rse.2022.113273
McGrane SJ (2016) Impacts of urbanisation on hydrological and water quality dynamics, and urban water management: a review. Hydrol Sci J 61:2295–2311. https://doi.org/10.1080/02626667.2015.1128084
McVittie A (2019a) Flood mapping using Snappy. Report. European Space Agency
McVittie A (2019b) Sentinel-1 flood mapping tutorial. Report
Merz B, Thieken AH, Gocht M (2007) Flood risk mapping at the local scale: concepts and challenges. In: Begum S, Stive MJF, Hall JW (eds) Flood Risk Management in Europe. Springer Netherlands, Dordrecht, pp 231–251
Minano A, Peddle S (2018) Using flood maps for community flood risk communication. Report prepared for Natural Resources Canada, Partners for Action, Waterloo, ON
Mohamadiazar N, Ebrahimian A, Hosseiny H (2024) Integrating deep learning, satellite image processing, and spatial-temporal analysis for urban flood prediction. J Hydrol 639:131508. https://doi.org/10.1016/j.jhydrol.2024.131508
Mudashiru RB, Sabtu N, Abustan I, Balogun W (2021) Flood hazard mapping methods: A review. J Hydrol 603:126846. https://doi.org/10.1016/j.jhydrol.2021.126846
Mukhopadhyay A, Pal I, Hati JP, et al (2024) High-resolution Pléiades data: an in-depth analysis of applications and future prospects. Spat Inf Res 32:739–755. https://doi.org/10.1007/s41324-024-00593-x
Munawar HS, Hammad AW, Waller ST (2022) Remote sensing methods for flood prediction: A review. Sensors 22:960. https://doi.org/10.3390/s22030960
Munyi JM (2024) The influence of urban morphology on flood susceptibility in slums in a data scarce

environment using machine learning. Info:eu-repo/semantics/masterThesis, University of Twente
Nazir U, Waseem MA, Khan FS, et al (2023) Improved flood mapping for efficient policy design by fusion of Sentinel-1, Sentinel-2 and Landsat-9 imagery to identify population and infrastructure exposed to floods. In: IGARSS 2023-2023 IEEE International Geoscience and Remote Sensing Symposium. IEEE, pp 1591–1594
Nguyen TH, Delmotte A, Fatras C, et al (2021) Validation and improvement of data assimilation for flood hydrodynamic modelling using SAR imagery data. arXiv
Nhangumbe M, Nascetti A, Ban Y (2023) Multi-temporal Sentinel-1 SAR and Sentinel-2 MSI data for flood mapping and damage assessment in Mozambique. Int J Geo-Inf 12:53. https://doi.org/10.3390/ijgi12020053
Nkwunonwo UC, Whitworth M, Baily B (2020) A review of the current status of flood modelling for urban flood risk management in the developing countries. Scientific African 7:e00269. https://doi.org/10.1016/j.sciaf.2020.e00269
Notti D, Giordan D, Caló F, et al (2018) Potential and limitations of open satellite data for flood mapping. Remote Sens 10:1673. https://doi.org/10.3390/rs10111673
Ogbonna WI (2023) Impact of poor drainage system and flood control in Nigeria (Anambra East Local Government Anam community as case study). Final year project, Nnamdi Azikiwe University
Olisoa FR (2012) Mutations des espaces périurbains d'Antananarivo: population, habitat et occupation du sol. PhD Thesis, Université de Strasbourg
O'Sullivan F (2022) The World's fastest-growing cities are facing the most climate risk. In: Bloomberg. https://www.bloomberg.com/news/articles/2022-02-28/global-south-cities-face-dire-climate-impacts-un-report. Accessed 30 Jan 2025
Papaioannou G, Vasiliades L, Loukas A (2015) Multi-criteria analysis framework for potential flood prone areas mapping. Water Resour Manage 29:399–418. https://doi.org/10.1007/s11269-014-0817-6
Park D, Markus M (2014) Analysis of a changing hydrologic flood regime using the Variable Infiltration Capacity model. J Hydrol 515:267–280. https://doi.org/10.1016/j.jhydrol.2014.05.004
Qiu J, Cao B, Park E, et al (2021) Flood monitoring in rural areas of the Pearl River Basin (China) using Sentinel-1 SAR. Remote Sens 13:1384. https://doi.org/10.3390/rs13071384
Quesada-Román A (2022) Disaster risk assessment of informal settlements in the Global South. Sustainability 14:10261. https://doi.org/10.3390/su141610261
Rahman M, Kamruzzaman M, Deb L, Islam HT (2024) Flood mapping, damage assessment, and susceptibility zonation in northeastern Bangladesh in 2022 using geospatial datasets. Prog Disaster Sci 100402. https://doi.org/10.1016/j.pdisas.2024.100402
Rahman MS, Di L (2017) The state of the art of spaceborne remote sensing in flood management. Nat Hazards 85:1223–1248. https://doi.org/10.1007/s11069-016-2601-9
Rakotoarimanana ZMH, Rakotovao SR (2022) Analysis of vulnerability and resilience of the population: case of flood in January 2022, in Antananarivo City, Madagascar
Rambinintsoa T (2012) Les contraintes hydrauliques de l'urbanisation d'Antananarivo
Ramiaramanana FN, Teller J (2021) Urbanization and floods in Sub-Saharan Africa: spatiotemporal study and analysis of vulnerability factors, case of Antananarivo agglomeration (Madagascar).

Water 13:149. https://doi.org/10.3390/w13020149
Ramiaramanana FN, Teller J, Sliuzas R, Kuffer M (2025) Using comparative approaches to model deprivation in Antananarivo, Madagascar: a multidimensional analysis using principal components analysis and weighting system across meso and macro scales. Habitat Int 159:103359. https://doi.org/10.1016/j.habitatint.2025.103359
Rentschler J, Salhab M, Jafino BA (2022) Flood exposure and poverty in 188 countries. Nat Commun 13:3527. https://doi.org/10.1038/s41467-022-30727-4
Saaty TL (2013) Analytic Hierarchy Process. In: Gass SI, Fu MC (eds) Encyclopedia of Operations Research and Management Science. Springer US, Boston, MA, pp 52–64
Sadiq R, Imran M, Ofli F (2023) Remote sensing for flood mapping and monitoring. In: Singh A (ed) International handbook of disaster research. Springer Nature Singapore, Singapore, pp 1–19
Saleh A, Yuzir A, Abustan I (2020) Flash flood susceptibility modelling: a review. In: IOP conference series: materials science and engineering. IOP Publishing, p 012005
Sar N, Ryngnga PK, De DK (2025) Application of the analytical hierarchy process (AHP) for flood susceptibility mapping using GIS techniques in lower reach of Keleghai River Basin, West Bengal, India. Geohazard Mech. https://doi.org/doi.org/10.1016/j.ghm.2025.06.002
Shamaoma H, Kerle N, Alkema D (2006) Extraction of flood-modelling related base-data from multi-source remote sensing imagery. In: Proceedings of the ISPRS Commission VII Symposium. International Institute for Geo-Information Science and Earth Observation, Enschede, The Netherlands
Shrestha MS, Takara K (2008) Impacts of floods in South Asia. Journal of South Asia Disaster Study 1:85–106
Sjöstrand K (2022) Urbanization impacts on floods. Nat Rev Earth Environ 3:738–738. https://doi.org/10.1038/s43017-022-00367-9
Sridhar KS, Mavrotas G (2021) Challenges of urbanization in the global south: introduction and overview. In: Urbanization in the Global South: perspectives and challenges. Routledge India, p 17
Suarez P (2002) Urbanization, climate change and flood risk: addressing the fractal nature of differential vulnerability. In: Proceedings of the Second Annual IIASA-DPRI Meeting: Integrated Disaster Risk Management – Megacity Vulnerability and Resilience. IIASA, Laxenburg, Austria, p 19
Tabari H (2020) Climate change impact on flood and extreme precipitation increases with water availability. Sci Rep 10:13768. https://doi.org/10.1038/s41598-020-70816-2
Tanim AH, McRae CB, Tavakol-Davani H, Goharian E (2022) Flood detection in urban areas using satellite imagery and machine learning. Water 14:1140. https://doi.org/10.3390/w14071140
Tarpanelli A, Mondini AC, Camici S (2022) Effectiveness of Sentinel-1 and Sentinel-2 for flood detection assessment in Europe. Nat Hazards Earth Syst Sci 22:2473–2489. https://doi.org/10.5194/nhess-22-2473-2022
Tavus B, Kocaman S, Nefeslioglu HA, Gokceoglu C (2020) A fusion approach for flood mapping using Sentinel-1 and Sentinel-2 datasets. Int Arch Photogramm Remote Sens Spatial Inf Sci XLIII-B3-2020:641–648. https://doi.org/10.5194/isprs-archives-XLIII-B3-2020-641-2020
Teng J, Jakeman AJ, Vaze J, et al (2017) Flood inundation modelling: a review of methods, recent advances and uncertainty analysis. Environ Model Softw 90:201–216.

https://doi.org/10.1016/j.envsoft.2017.01.006
Twele A, Cao W, Plank S, Martinis S (2016) Sentinel-1-based flood mapping: a fully automated processing chain. Int J Remote Sens 37:2990–3004. https://doi.org/10.1080/01431161.2016.1192304
Uddin K, Matin MA, Meyer FJ (2019) Operational flood mapping using multi-temporal Sentinel-1 SAR images: a case study from Bangladesh. Remote Sens 11:1581. https://doi.org/10.3390/rs11131581
Van den Bout B, Jetten VG, van Westen CJ, Lombardo L (2023) A breakthrough in fast flood simulation. Environ Model Softw 168:105787. https://doi.org/10.1016/j.envsoft.2023.105787
Vojtek M, Vojteková J (2018) Flood maps and their potential role in local spatial planning: a case study from Slovakia. Water Policy 20:1042–1058. https://doi.org/10.2166/wp.2018.077
Watson CS, Gyawali J, Creed M, Elliott JR (2024) City-scale high-resolution flood models and the role of topographic data: a case study of Kathmandu, Nepal. Geocarto Int 39:2387073. https://doi.org/10.1080/10106049.2024.2387073
Williams DS, Máñez Costa M, Celliers L, Sutherland C (2018) Informal settlements and flooding: identifying strengths and weaknesses in local governance for water management. Water 10:871. https://doi.org/10.3390/w10070871
Wu C-F, Chen S-H, Cheng C-W, Trac LVT (2021) Climate justice planning in global south: applying a coupled nature–human flood risk assessment framework in a case for Ho Chi Minh City, Vietnam. Water 13:2021. https://doi.org/10.3390/w13152021
Yésou H, Escudier A, Battiston S, et al (2015) Exploitation de l'imagerie Pléiades-THR en cartographie réactive suite à des catastrophes naturelles ayant affecté le territoire français en 2013. Rev Fr Photogramm Télédétect 39–45. https://doi.org/10.52638/rfpt.2015.210
Zakaria SF, Zin RM, Mohamad I, et al (2017) The development of flood map in Malaysia. In: AIP Conference Proceedings. AIP Publishing, p 110006
Zhao H (2005) A fast sweeping method for eikonal equations. Math Comput 74:603–627. https://doi.org/10.1090/S0025-5718-04-01678-3